

Electronic Supplementary Information (ESI)

Ligand-Mediated Reversal of the Oxidation state Dependent ROS Scavenging and Enzyme Mimicking Activity of Ceria Nanoparticles

Vaishwik Patel,^a Mandeep Singh,^b Edwin L. H. Mayes,^c Abraham Martinez,^d Vaithiyalingam Shutthanandan,^d Vipul Bansal,^b Sanjay Singh,^a and Ajay S. Karakoti^{*a,e}

^aBiological and Life Sciences, School of Arts and Sciences, Ahmedabad University, Ahmedabad, Gujarat, 380009 India

^bIan Potter NanoBioSensing Facility, NanoBiotechnology Research Laboratory, School of Science, RMIT University, Melbourne, VIC, 3000, Australia

^cRMIT Microscopy and Microanalysis Facility, RMIT University, Melbourne, VIC, 3000, Australia

^dEnvironmental and Molecular Sciences Laboratory, Pacific Northwest National Laboratory, Richland, WA – 99354, USA

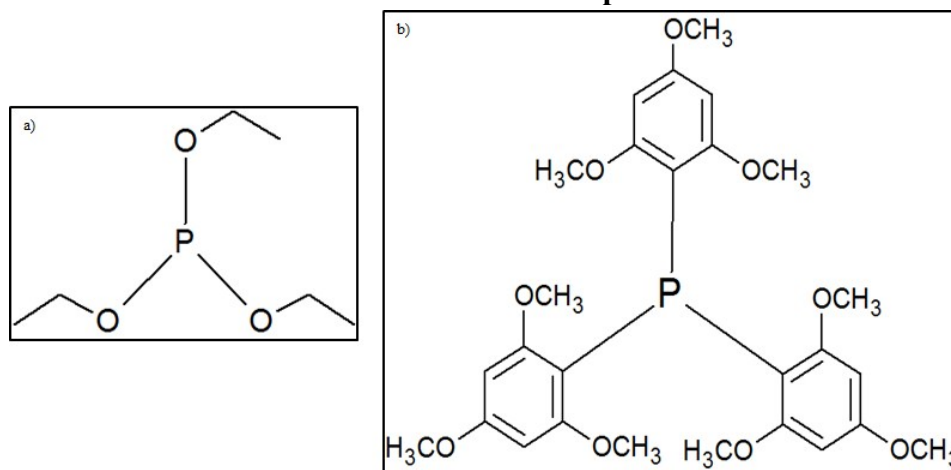
^eSchool of Engineering and Applied Science, Ahmedabad University, Ahmedabad, Gujarat, 380009 India

*Corresponding author – ajay.karakoti@ahduni.edu.in

Table of content for Electronic Supplementary Information (ESI)

ESI-I Structure of Phosphines	2
ESI- II Materials and Methods	2
ESI-IIa Nanoparticles synthesis	2
ESI-IIb Surface modification of bare nanoceria	3
ESI-IIc Characterization of bare and functionalized nanoceria	3
ESI-IId Photoluminescence activity.....	4
ESI-IIe Superoxide dismutase (SOD) mimetic activity	4
ESI-IIf Catalase mimetic activity.....	4
ESI-IIg X-ray photoelectron spectroscopy (XPS)	5
ESI- III Tables	6
ESI- IV Figures	7
ESI X References	13

ESI-I Structure of Phosphines



Scheme 1. Structure of phosphines a), TEP, b) TTMPP

ESI- II Materials and Methods

Ammonium cerium nitrate, Cerium nitrate hexahydrate, TEP, TTMPP, Xanthine oxidase, Hypoxanthine, Catalase, Tris HCl and Dialysis tube (MWCO:- 6-8 kDa) were purchased from Sigma Aldrich, Amplex red assay kit was purchased from Invitrogen, Hydrogen peroxide (H₂O₂), NH₄OH and DTPA (diethylenetri-aminepentaacetic acid) were obtained from S D Fine Chem. Limited. Vivaspin® 20 (20 KDa concentrators) were purchased from Sartorius. All glassware was washed following a stringent protocol of acid wash, alkali wash, detergent wash, tap water rinse, distilled water rinse and a final DI water rinse to make it free from all impurities and ions. After this procedure, the glassware was further rinsed with hot piranha solution to remove organic contaminants. The glassware was washed and used as and when needed. The nanoparticles (NPs) were stored in several small aliquots at room temperature in ambient laboratory conditions and were found to be stable for up to one year (duration of the current study).

ESI-IIa Nanoparticles synthesis

CeO_{2-x} NPs were synthesized by wet chemical method followed by ambient temperature ageing for 15-21 days¹. The predominance of Ce³⁺ oxidation state was observed by the transformation of the solution from yellow to colourless and confirmed by UV-visible spectroscopy (figure 1). pH

of the solution was maintained at 3. CeO₂ NPs were synthesized by the thermal hydrolysis method from hydrolysis of ammonium Ce(IV) nitrate using NH₄OH (5 N) at 70 degrees². Resulting particles were approximately around 8-12 nm. pH of the solution was 3 after dialysis.

ESI-IIb Surface modification of bare nanoceria

CeO₂-x (5 mM) or CeO₂ (10 mM) nanoparticles were mixed with TEP or TTMPP (separately) for the preparation of TEP and TTMPP functionalized particles of cerium oxide nanoparticles respectively by string for 2 hours and then leave it for overnight. TEP and TTMPP solutions were prepared in deionized water. For dissolution of TTMPP the pH of the water was adjusted to 3 because of water insolubility of TTMPP at normal pH. Equimolar concentration of ligands was used for functionalization (5 mM TEP and TTMPP for functionalization with CeO₂-x and 10 mM TEP and TTMPP for functionalization with CeO₂). The samples were stirred for 2 hours after mixing. The samples were then incubated overnight without any stirring at ambient laboratory conditions. TEP conjugated nanoparticles (CeO₂-x-TEP or CeO₂-TEP) were purified (removal of unbound ligands) by extensive dialysis through 6-8 kDa dialysis membrane. The dialysis was monitored through pH.

Sample	Unpurified	purified
CeO ₂ -x-TEP	3.49	3.602
CeO ₂ -x-TTMPP	2.7	3.18
CeO ₂ -TEP	2.985	3.125
CeO ₂ -TTMPP	2.564	3.445

Due to instability of TTMPP conjugated nanoparticles (CeO₂-x-TTMPP or CeO₂-TTMPP) during dialysis these samples were purified by washing through 20 kDa concentrators. The supernatant was measured for by UV-Vis to ensure that all unbound TTMPP was removed.

ESI-IIc Characterization of bare and functionalized nanoceria

UV-visible spectrum was analyzed by PerkinElmer LAMBDA 365 spectrofluorometer with help of quartz cuvette having 1.0 cm path length. Zeta potential measurements were carried out using Malvern zeta sizer nano ZS with dip cell probe. TEM images were collected by using Jeol JEM1400 plus operating at 120 keV and samples were prepared on 200 mesh copper grid coated with a thin layer of carbon. FT-IR spectrum for functional group detection was analyzed by PerkinElmer Spectrum Two. Confocal Raman spectra were acquired on a Horiba LabRAM HR

Evolution micro-Raman spectrometer using a 532 nm laser, 5 mW laser power, 1 sec exposure, average of 20 accumulated spectra and a 100× objective, as described previously³. HR-TEM images were obtained on a JEOL 2100F microscope operating at 200 kV accelerating voltage. EDS was performed in STEM mode on a JEOL 2100F instrument.

ESI-II d Photoluminescence activity

PL spectra measurements were done using Agilent Cary Eclipse fluorescence spectrometer. PL activity of functionalized nanoceria was measured by the addition of a different volume of phosphine into nanoceria. PL activity was measured at excitation wavelength 255nm and PMT was kept at 600 V for all the measurement. Bare CeO_{2-x} was titrated by incremental addition of TEP (100 µl) and TTMPP (10 µl) till the saturation or quenching was observed respectively.

ESI-II e Superoxide dismutase (SOD) mimetic activity

SOD mimetic activity was measured by the method described by Korsvik et al⁴. Reduction of ferricytochrome C induced by superoxide radicals produced by the reaction of xanthine oxidase/hypoxanthine system. Bare and modified NPs neutralize the superoxides and prevent cytochrome C reduction. Reduction of Cytochrome C was analyzed at 550 nm in 96 well plates with a 100 µL final volume using a Spectramax 190 UV-visible spectrophotometer (Molecular Devices, Sunnyvale, CA). Catalase was added to remove hydrogen peroxide, a byproduct of SOD activity. The SOD activity for CeO_{2-x} nanoparticles before and after functionalization was measured at a concentration of 0.1 mM while that of CeO₂ nanoparticles was measured at 0.2 mM. As CeO₂ NPs has limited SOD activity its concentration needs to be increased to observe the effect of functionalization on its SOD activity.

ESI-II f Catalase mimetic activity

Catalase mimetic activity of nanoceria was analyzed by using Amplex Red Hydrogen Peroxide/Peroxidase assay kit (Invitrogen, Eugene, Oregon), which is used for the measurement of qualitative and quantitative measurement of H₂O₂ concentration. The Amplex Red reagent dissolved in DMSO, in presence of horseradish peroxidase (HRP) reacts with H₂O₂ and generate fluorophore resorufin. The study was performed in 0.25 M sodium phosphate buffer solution. Resorufin obtained as a result of oxidation of Amplex Red reagent by H₂O₂ analyzed at 560 nm in Eppendorf spectrofluorometer. Standard curve of H₂O₂ generated by using the method described in the kit. Samples containing Amplex Red reagents and NPs were taken at every 10 minutes and

assayed in 96 well plates for quantitative analysis of resorufin generation. The final concentration of H₂O₂ in each sample at the beginning of the reaction was 25 μM⁵.

ESI-IIg X-ray photoelectron spectroscopy (XPS)

XPS measurements were recorded using Kratos Axis Ultra spectrophotometer using a monochromatic focused Al Kα x-ray (1486.7 eV) source. For XPS measurements 15uL of sample solution was dropped on a pre-cleaned silicon wafer and dried in the load lock chamber. The sample was seamlessly transferred from the load lock chamber to the main chamber for measurements. The base pressure of the main chamber was maintained at 5.2×10^{-9} torr and it reduced to 2.6×10^{-8} torr after inserting the NPs sample for XPS measurements. The charging shifts were referenced to 916.6eV peak from cerium 3d_{3/2} core level peak. The survey spectra were collected at 160eV pass energy and the high-resolution scans for individual elements were collected at pass energy of 40eV with 0.1eV step size at a dwell time of 300 seconds. Binding energy of the instrument was calibrated prior to sample characterization and referenced to an energy scale with binding energies for Cu 2p_{3/2} at 932.67±0.05 eV and Au 4f at 84.0±0.05 eV.

ESI- III Tables

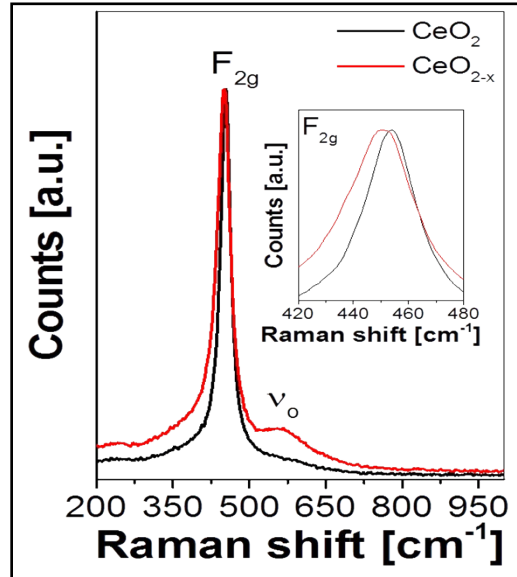
ESI-IIIa. Zeta potential of bare and functionalized nanoceria

Sample Name	First Reading (mV)	Second Reading (mV)	Third Reading (mV)
CeO _{2-x}	53.4	58.3	55.6
CeO ₂	59.5	60.4	59.6
CeO _{2-x} -TEP	3.12	3.42	3.39
CeO _{2-x} -TTMPP	38.0	41.0	42.5
CeO ₂ -TEP	14.7	16.6	16.1
CeO ₂ -TTMPP	29.4	30.6	31.1

ESI-IIIb. Peak fitting Cerium Oxide

Assigned Peak	Charge State	Referenced peak Position	CeO _{2-x}		CeO ₂		CeO _{2-x} -TEP		CeO _{2-x} -TTMPP		CeO ₂ -TEP		CeO ₂ -TTMPP	
			FWHM	Peak %	FWHM	Peak %	FWHM	Peak %	FWHM	Peak %	FWHM	Peak %	FWHM	Peak %
v	Ce 4+	882.43	2.65	15.61	2.25	21.06	2.65	11.85	2.65	12.55	2.25	17.89	2.25	18.16
v''	Ce 4+	888.61	5.65	0.28	4.25	16.16	3.25	2.38	5.65	0.71	4.11	11.28	3.82	12.57
u0	Ce 3+	899.20	2.25	2.99	2.62	0	2.65	2.53	2.29	2.93	2.65	1.29	2.25	1.1
v'	Ce 3+	884.73	3.42	37.44	2.55	5.21	3.5	31.76	3.25	36.79	3.35	16.19	3.5	13.81
u	Ce 4+	900.98	2.16	7.49	1.69	10.87	2.85	10.37	2.64	8.61	2	10.14	2	10.2
u''	Ce 4+	907.50	3.18	3.43	3.5	7.35	2.95	3.17	2.55	1.88	3.24	5.16	2.98	5.09
u'''	Ce 4+	916.70	2.59	2.65	2.25	14.96	2.25	1.98	2.07	1.44	2.05	10.19	2.32	12.57
u'	Ce 3+	903.20	3.46	22.55	2.55	2.72	3.5	20.36	3.5	24.14	3.29	9.15	3.45	5.66
v0	Ce 3+	880.40	2.55	3.42	2.65	0	2.65	8.99	2.55	7.94	2.55	2.34	2.55	2.22
v'''	Ce 4+	896.30	2.65	4.15	2.19	21.68	2.65	6.6	2.65	3.01	2.25	16.37	2.33	18.62
Total Ce3+ (%)			66.4		7.93		63.64		71.8		28.97		22.79	

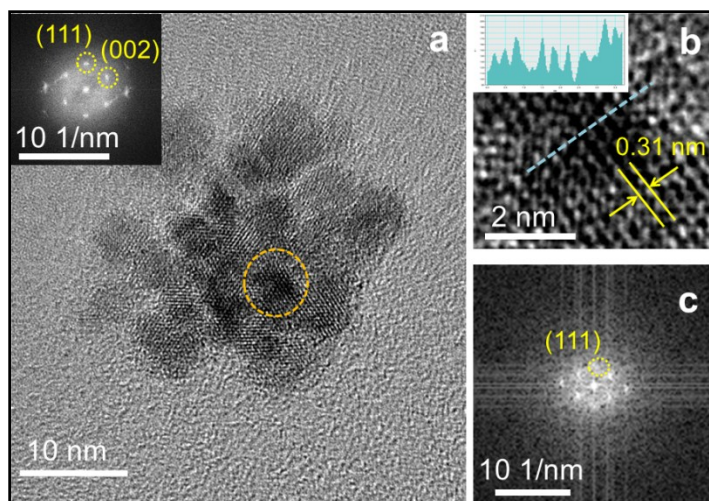
ESI- IV Figures



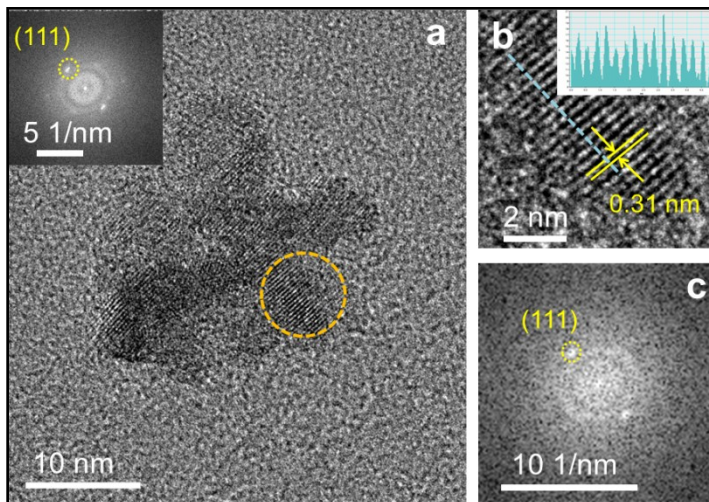
ESI-IVa. Raman spectra of pristine CeO_2 and CeO_{2-x} nanoparticles. The inset shows the expanded region of the F_{2g} mode, depicting peak-shifts and broadening of the Raman mode. Signatures corresponding to oxygen-deficient states in CeO_{2-x} particles are represented as v_o . The predominant Raman active phonon mode F_{2g} in both these materials is attributed to a symmetrical stretching mode of O anions around Ce cations (O–Ce–O) in the cubic lattice. The F_{2g} mode in bulk stoichiometric CeO_2 appears as a sharp peak at ca. 465 cm^{-1} .⁶ This mode is highly sensitive to any disorder in the oxygen sub lattice caused by thermal and/or grain size-induced non-stoichiometry. The broadening of this peak along with blue shift from the bulk is attributed to the reduction in the phonon lifetime in the nanocrystalline regime. The blue shift of the F_{2g} mode of 11 and 14 cm^{-1} in our CeO_2 and CeO_{2-x} particles, respectively, along with their broadness is notable. This broadening can be described by the dependence of the half-width Γ on the inverse of grain size d_g , and can be used to calculate the grain size, as follows a linear behaviour (equation 1).

$$\Gamma (\text{cm}^{-1}) = 10 + \frac{124.7}{d_g} \quad (1)$$

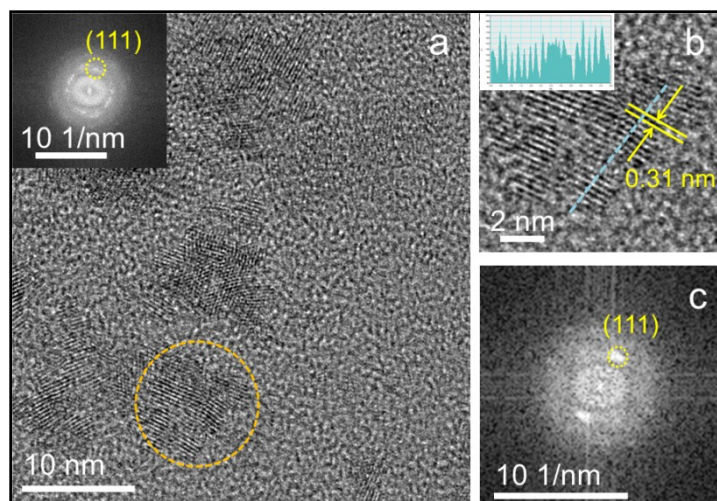
As such, Raman studies revealed the crystallite sizes of 5.8 and 3.9 nm for CeO_2 and CeO_{2-x} , respectively that corroborate well with the HRTEM studies. Further, in contrast to CeO_2 nanoparticles, the oxygen deficient nanoparticles (CeO_{2-x}) showed an additional well-defined feature at ca. 590 nm, which is indicative of the presence of oxygen vacancies (v_o) in the ceria lattice.



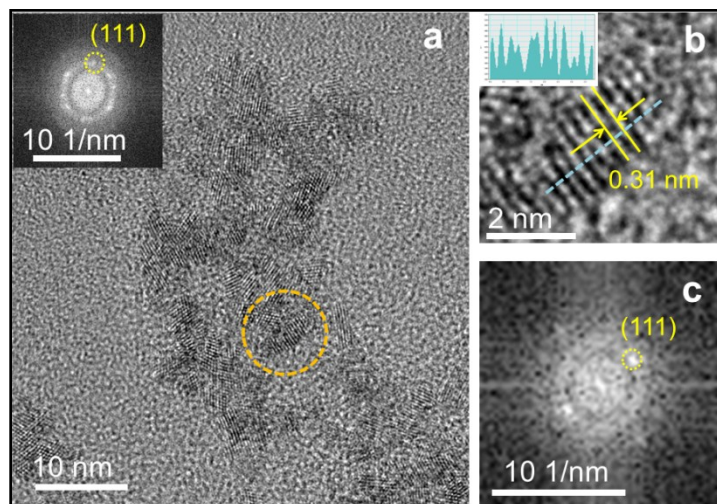
ESI-IVb. HR-TEM data of pristine CeO_{2-x} nanoparticles. (a) HR-TEM image of a cluster of particles along with corresponding reduce fast Fourier transform (FFT) pattern shown in the inset, (b) lattice-resolved image of the particle highlighted in (a) along with the corresponding lattice fringe distribution in the inset showing inconsistent lattice planes in certain regions of the particles representative of defect-rich regions, and (c) the reduce FFT pattern from the single particle shown in (b).



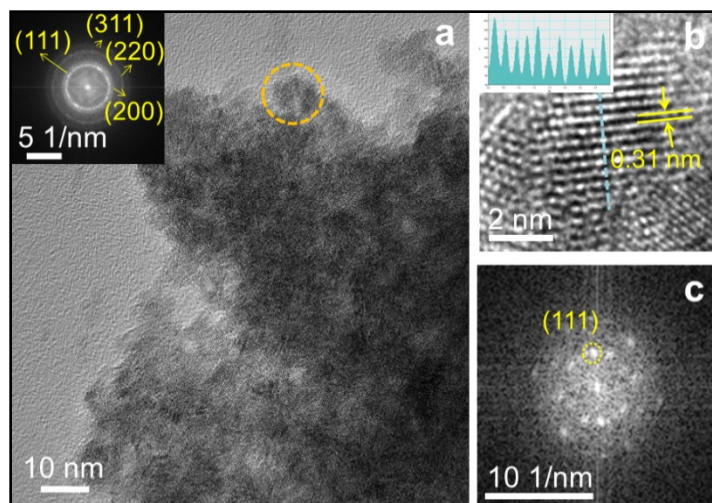
ESI-IVc. HR-TEM data of pristine CeO₂ nanoparticles. (a) HR-TEM image of a cluster of particles along with corresponding reduce fast Fourier transform (FFT) pattern shown in the inset, (b) lattice-resolved image of the particle highlighted in (a) along with the corresponding lattice fringe distribution in the inset showing consistent lattice planes without any defects, and (c) the reduce FFT pattern from the single particle shown in (b).



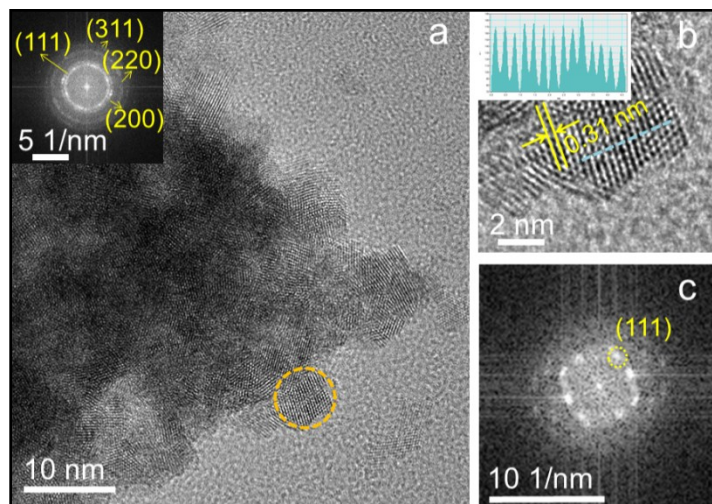
ESI-IVd. HR-TEM data of CeO_{2-x} nanoparticles coated with TEP. (a) HR-TEM image of a cluster of particles along with the corresponding reduce fast Fourier transform (FFT) pattern shown in the inset, (b) lattice-resolved image of the particle highlighted in (a) along with the corresponding lattice fringe distribution in the inset showing a mixture of consistent lattice planes without any defects and defect-rich regions, and (c) the reduce FFT pattern from the single particle shown in (b).



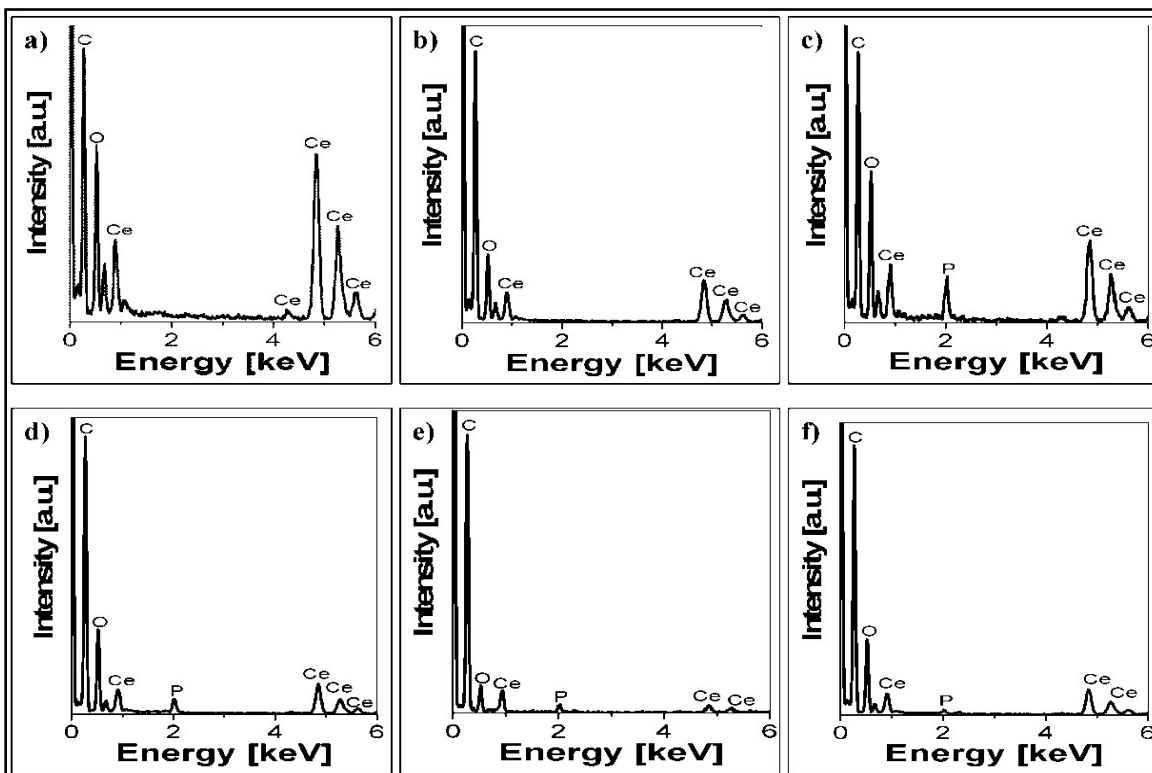
ESI-IVe. HR-TEM data of CeO_{2-x} nanoparticles coated with TTMPP. (a) HR-TEM image of a cluster of particles along with corresponding reduce fast Fourier transform (FFT) pattern shown in the inset, (b) lattice-resolved image of the particle highlighted in (a) along with the corresponding lattice fringe distribution in the inset showing a mixture of consistent lattice planes without any defects along with defect-rich regions, and (c) the reduce FFT pattern from the single particle shown in (b).



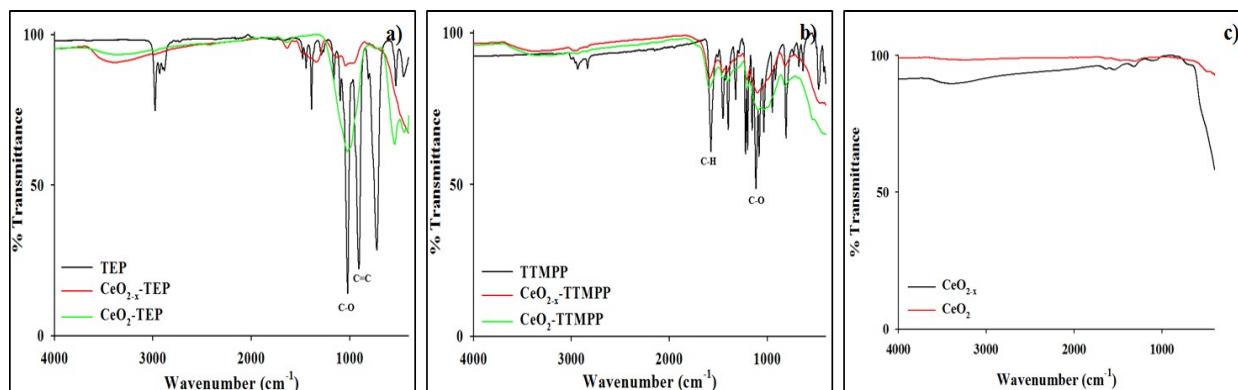
ESI-IVf. HR-TEM data of CeO₂ nanoparticles coated with TEP. (a) HR-TEM image of a cluster of particles along with corresponding reduce fast Fourier transform (FFT) pattern shown in the inset, (b) lattice-resolved image of the particle highlighted in (a) along with the corresponding lattice fringe distribution in the inset showing consistent lattice planes without any defects, suggesting that the TEP coating does not influence the original crystallinity of the particles, and (c) the reduce FFT pattern from the single particle shown in (b).



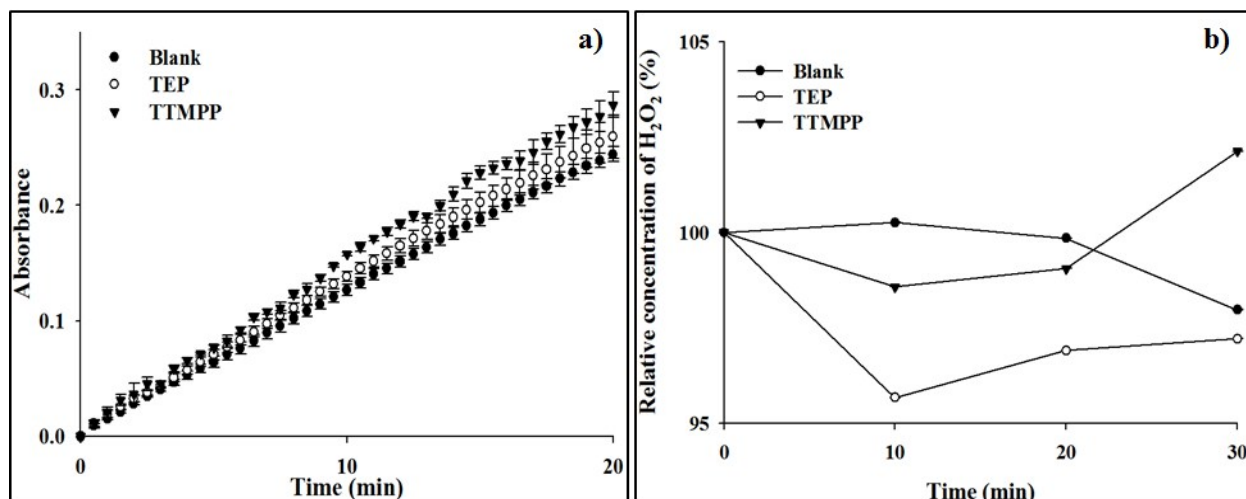
ESI-IVg. HR-TEM data of CeO₂ nanoparticles coated with TTMPP. (a) HR-TEM image of a cluster of particles along with the corresponding reduce fast Fourier transform (FFT) pattern shown in the inset, (b) lattice-resolved image of the particle highlighted in (a) along with the corresponding lattice fringe distribution in the inset showing consistent lattice planes without any defects, suggesting that TTMPP coating does not influence the original crystallinity of the particles, and (c) the reduce FFT pattern from the single particle shown in (b).



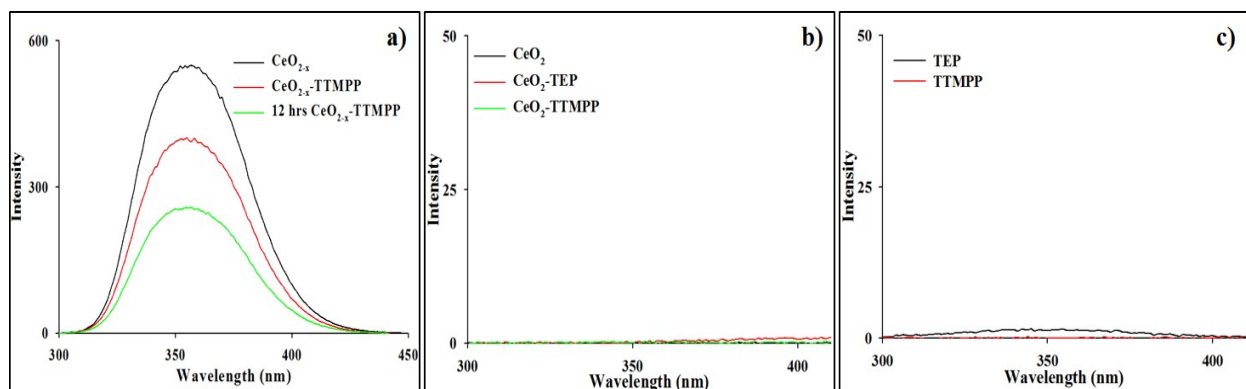
ESI-IVh. EDX pattern from specific locations indicated in the TEM images of a) CeO₂ b) CeO_{2-x} c) CeO₂-TEP d) CeO₂ TTMPP e) CeO_{2-x} TEP and f) CeO_{2-x} TTMPP samples depicting the successful surface functionalization of both types of cerium oxide nanoparticles. Small phosphorus signal in TTMPP samples relative to the corresponding TEP samples points to the bulky nature of TTMPP molecule.



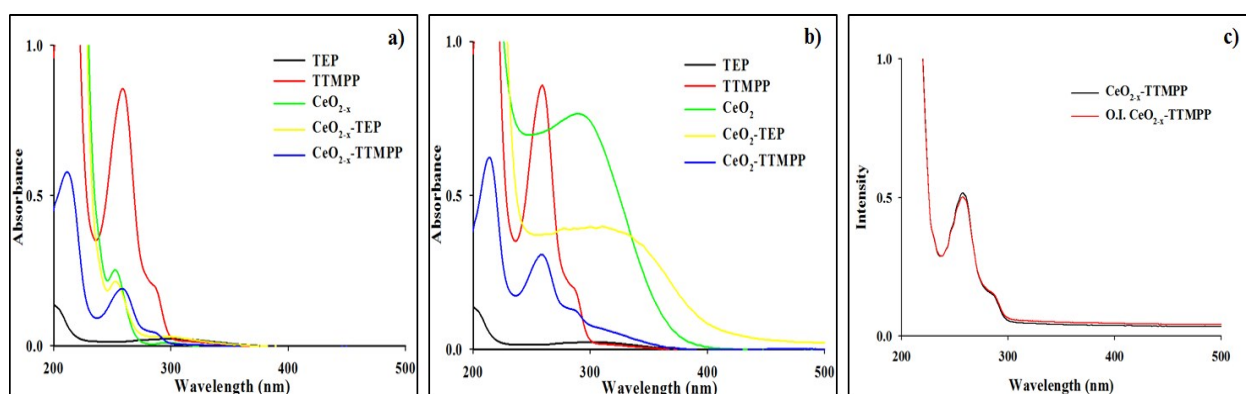
ESI-IVi. FT-IR spectra of a) TEP prior to and after functionalization, b) TTMPP prior to and after functionalization and c) Bare ceria nanoparticles.



ESI-IVj. Enzymatic activity tests for pure phosphines depict the absence of activity a) SOD and b) Catalase mimetic activity



ESI-IVk. Photoluminescence plots of bare and functionalized, a) PL titration experiments were conducted at molar ratio of (CeO_{2-x} :TTMP 25:3), b) bare and phosphine functionalized CeO_2 nanoparticles 3) Plain phosphines.



ESI-IVl. UV-Visible spectra of bare phosphines and a) CeO_{2-x} , b) CeO_2 NPs functionalized with phosphines and c) comparative spectra of freshly prepared and overnight incubated (O.I.) CeO_{2-x} functionalized with TTMP functionalized with TTMP.

ESI X References

1. A. S. Karakoti, S. V. N. T. Kuchibhatla, K. S. Babu and S. Seal, *The Journal of Physical Chemistry C*, 2007, **111**, 17232-17240.
2. A. Sehgal, Y. Lalatonne, J.-F. Berret and M. Morvan, *Langmuir*, 2005, **21**, 9359-9364.
3. S. Mandeep, G. Enrico Della, A. Taimur, W. Sumeet, R. Rajesh, E. Joel van, M. Edwin and B. Vipul, *2D Materials*, 2017, **4**, 025110.
4. C. Korsvik, S. Patil, S. Seal and W. T. Self, *Chemical Communications*, 2007, 1056-1058.
5. T. Pirmohamed, J. M. Dowding, S. Singh, B. Wasserman, E. Heckert, A. S. Karakoti, J. E. S. King, S. Seal and W. T. Self, *Chemical communications (Cambridge, England)*, 2010, **46**, 2736-2738.
6. P. Kumar, P. Kumar, A. Kumar, I. Sulania, F. Chand and K. Asokan, *RSC Advances*, 2017, **7**, 9160-9168.